



## Performance of fluoride electrosorption using micropore-dominant activated carbon as an electrode



Yingzhen Li, Yanping Jiang, Ting-Jie Wang\*, Chang Zhang, Haifeng Wang

Department of Chemical Engineering, Tsinghua University, Beijing 100084, China

### ARTICLE INFO

#### Article history:

Received 20 April 2016

Received in revised form 25 August 2016

Accepted 31 August 2016

Available online 01 September 2016

#### Keywords:

Electrosorption

Fluoride removal

Adsorption

Charge efficiency

Activated carbon

### ABSTRACT

Fluoride electrosorption using micropore-dominant activated carbon (AC) as an electrode was developed. The parameters of voltage, flow rate, and electrode gap were optimized to be 1.6 V, 10 mL/min and 2 mm, respectively. The electrosorption isotherm conforms to the Langmuir model, indicating the monolayer adsorption of the fluoride ions. The saturated electrosorption capacity for fluoride ions under the optimized parameters was 16.8 mg/g (AC). The high saturated electrosorption capacity of this micropore-dominant AC was attributed to its high specific surface area of 2130 m<sup>2</sup>/g, which was mainly contributed by the micropores. The saturated electrosorption capacity has a linear relationship to the square of the applied voltage. The fluoride electrosorption occurred only when the voltage was higher than the electro-capillary maximum voltage of 0.14 V for this AC. The charge efficiency reached a high value of 0.98 for the micropore-dominant AC, indicating that only counterions existed in the micropores.

© 2016 Elsevier B.V. All rights reserved.

### 1. Introduction

Fluorine is an essential trace element for the human body and helpful to enhance bone and tooth strength. However, excessive intake of fluoride will cause damage to the human body [1,2]. The fluoride that enters the human body mainly comes from drinking water, and the fluoride concentration limit of the World Health Organization (WHO) is 0.5–1.5 mg/L [3]. However, the fluoride concentration in groundwater is often much higher than this value [4]. The chronic intake of drinking water containing excessive fluoride will lead to dental and skeletal fluorosis [5,6], so fluoride removal from drinking water is very important.

Adsorption is the most widely used method, and a large number of adsorbents have been synthesized for fluoride removal from drinking water [7]. Cost-effective adsorbents such as diatomaceous earth, bone char, and zeolites [8], usually have low adsorption capacity. Compared with natural adsorbents, metal oxide adsorbents, such as nano-alumina [9] and granular ferric hydroxide [10], have higher adsorption capacity. To further increase the adsorption capacity, composite metal adsorbents such as Fe-Ti [11], Fe-Zr [12], and Fe-Cr [13] have been synthesized. Expensive rare earth metals are also often used for increasing the adsorption capacity, such as Fe-Al-Ce [14], Ce-Ti [15], Mn-Ce [16], which entails a high cost.

Practically, cheap adsorbents usually suffer from low adsorption capacity [12], and the high-capacity adsorbents usually suffer from high costs. In addition, the regeneration of the adsorbents introduces an additional cost. Because the fluoride is usually chemically adsorbed on the adsorbents, alkali washing is usually used to remove the adsorbed fluoride, followed by acid washing to neutralize the pH in the regeneration solution. This not only increases the costs but also produces more waste water and causes secondary pollution to the environment. Metal adsorbents are also inevitably dissolved into water in the fluoride adsorption process, causing ion pollution of the water [17].

Electrosorption is a clean and economical method that generates no secondary pollution [18]. Carbon materials with a high specific surface area, such as activated carbon (AC) [19–21], carbon fibers [22,23], carbon aerogels [24], carbon nanotubes [25], graphene [26,27], mesoporous carbon [28], and carbon composite materials [29,30], have been used to produce electrodes for electrosorption. After applying a voltage, the two electrodes are positively and negatively charged, respectively. When aqueous solution flows through the gap between the electrodes, cations move to the negative electrode and anions move to the positive electrode under the action of the electric field, forming an electric double layer on the electrode surface. The ions in the solution are gradually moved onto the electrode surface and stored in the electric double layer, decreasing the bulk concentration of the solution [31]. Upon shorting the electrodes, the adsorbed ions are released back into the bulk solution, which causes the electrodes to be

\* Corresponding author.

E-mail address: [wangtj@tsinghua.edu.cn](mailto:wangtj@tsinghua.edu.cn) (T.-J. Wang).

regenerated. Electrosorption is a non-Faradaic process, and the ions are fixed by the Coulomb force instead of chemical bonds on the electrode surface, so acid or alkali washing is not needed for the regeneration of the electrodes [21].

Electrosorption has the advantages of high energy efficiency, high removal efficiency, low cost and easy regeneration. Electrosorption has been studied in many works for removing NaCl [21,28,32] and other ions such as  $\text{Cr}^{2+}$  [33],  $\text{Cu}^{2+}$  [34],  $\text{Fe}^{3+}$  [35], and  $\text{NO}_3^-$  [36]. However, there have been few reports on fluoride removal by electrosorption. Tang et al. [37] studied the fluoride and nitrate removal from water by electrosorption using the activated carbon electrodes, the energy consumption was calculated by assuming the charge efficiency as 1. Some similar research about desalination using the activated carbon electrodes indicated the charge efficiency was below 0.5 [38]. The charge efficiency directly affects the energy consumption, which needs to be studied. The applied voltage is the key parameter in the electrosorption, and higher applied voltage leads to higher desalting capacity due to stronger electrostatic interaction. Hou et al. reported that the removal efficiency of ferric ions increased with the applied voltage below 2.0 V. However, when the electrical voltage was increased to 2.2 V, the removal efficiency gradually decreased due to the electrolysis of water [35]. The electrolysis of water was also observed at an applied voltage of 1.4 V in other report [19].

AC is widely used to produce electrodes due to its large specific surface area and low cost. The high specific surface area brings a high electrical double-layer capacitance, which results in a high electrosorption capacity [39]. Han et al. also reported that the AC electrode with the higher micropore porosity and specific surface area was preferable to obtain the higher electrosorption capacity [38]. In this paper, a micropore-dominant AC with narrow pore size was used as the electrode material. The effects of the applied voltage on the electrosorption capacity were studied. The applied voltage, flow rate, and electrode gap were optimized for high electrosorption efficiency. The electrosorption mechanism was studied by analyzing the electrosorption isotherm and the charge efficiency.

## 2. Materials and methods

### 2.1. Fabrication of AC electrode

AC with a specific surface area of  $2130 \text{ m}^2/\text{g}$  (Fuzhou Yi-Huan Carbon, China) was used as the electrode material. To fabricate the carbon electrode, a carbon slurry was prepared by mixing AC powder, carbon black (Fuzhou Yi-Huan Carbon, China), and the solution of poly(vinylidene fluoride) (PVDF, MW = 275,000, Sigma-Aldrich, USA) dissolved in di-methylacetamide (DMAC, Beijing Chemical Reagents, China). The slurry was stirred for 3 h to ensure homogeneity and then coated on a graphite plate. The coated plate was dried in an oven at  $80^\circ\text{C}$  for 6 h and then put in a vacuum oven at  $50^\circ\text{C}$  for 2 h to completely remove the organic solvent remaining in the micropores of the coated layer. The obtained AC electrode consists of 80% AC, 10% carbon black as conductive material, and 10% PVDF as binder. The AC electrodes were then assembled into an electrosorption cell.

### 2.2. Characterization of AC electrode

The Brunauer-Emmett-Teller (BET) surface area and pore size distribution (PSD) were measured by nitrogen adsorption at 77 K using a surface area analyzer (Autosorb-iQ, Quantachrome Instruments USA). The PSD was calculated by density functional theory (DFT) from the adsorption isotherm.

An electrochemical workstation (CHI 600 D, Shanghai CH Instrument Company, China) with a three-electrode system was used to analyze the characteristics of the capacitance, electrical adsorption, and desorption of the fabricated carbon electrode. The carbon electrode was fixed as the working electrode, and a platinum electrode and Ag/AgCl electrode were used as the counter and reference electrodes, respectively. 1.0 M NaCl solution was used as the electrolyte, and the water temperature in all measurements were kept at  $25^\circ\text{C}$ . The cyclic voltammetry (CV) performance was measured at different scan rates from 1 to 50 mV/s, and the electrical potential range was set from  $-0.6 \text{ V}$  to  $0 \text{ V}$  (vs Ag/AgCl electrode). The capacitance was calculated from the current-voltage curves according to Eq. (1),

$$C = \frac{\int IdV}{\nu mV} \quad (1)$$

where  $C$  is the specific capacitance ( $\text{F/g(AC)}$ ),  $I$  is the response current (A),  $V$  is the instantaneous potential (V),  $\nu$  is the scan rate of the electrical potential (V/s), and  $m$  is the mass of AC on the electrodes (g) in this work.

### 2.3. Electrosorption apparatus and experiments

A schematic diagram of the electrosorption cell is shown in Fig. 1. The AC electrode had a size of  $60 \times 60 \times 0.2 \text{ mm}$ , and a hole with a diameter of 6 mm was opened for water to flow through. An insulated spacer was used to separate the two electrodes to avoid short circuits and also as a water flow path. The electrodes were fixed using a Plexiglas plate, and both of them had a hole with a diameter of 6 mm for water to flow through.

A stock solution with a fluoride concentration of 500 mg/L was prepared using NaF reagent (AR, Beijing Chemical Reagents, China) and deionized water and was diluted to different concentrations. The fluoride concentration of the effluent was measured using a conductivity meter, and the correlation of the conductivity ( $\mu\text{S}/\text{cm}$ ) to the concentration (mg/L) was calibrated prior to the experiment. The conductivity of the fluoride solution had an excellent linear relationship with the fluoride concentration. Before each

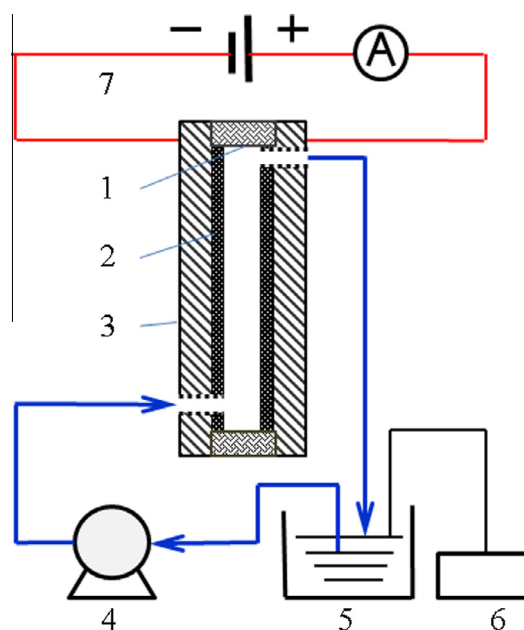


Fig. 1. Schematic diagram of the experimental apparatus 1. insulated spacer; 2. AC electrode; 3. graphite plate; 4. peristaltic pump; 5. feed tank; 6. conductivity meter; 7. potentiostat.

experiment, the cell was washed with deionized water to remove any dissolved salts from the experimental system for precise measurement of the water conductivity. In the electrosorption process, the fluoride solution was fed through a peristaltic pump into the electrosorption cell, and then the effluent returned to the feed tank and the solution was circulated until reaching the electrosorption equilibrium. In the optimization of the applied voltage and flow rate, the volume of the solution was set to 50 mL, and the temperature was set to 25 °C. The applied voltage was adjusted by a potentiostat. To avoid electrolysis, the voltage range was maintained below 1.6 V, where no water electrolysis was observed. A flow rate range of 1–20 mL/min was used in the optimization.

The equilibrium electrosorption capacity is defined as

$$Q(\text{mg/g}) = \frac{(C_0 - C_e)V}{m} \quad (2)$$

where  $Q$  is the equilibrium electrosorption capacity (mg/g (AC)),  $C_0$  and  $C_e$  (mg/L) are the initial and equilibrium concentrations of fluoride, respectively,  $V$  is the volume of the circulated solution (L), i.e., 50 mL in this work, and  $m$  is the AC mass on the electrode (g), i.e., 0.18 g.

### 3. Results and discussion

#### 3.1. Characteristics of AC electrode

The  $N_2$  adsorption isotherm of AC is shown in Fig. 2. The adsorption quickly reached saturation at a low relative pressure, which is the typical type I pattern from the classification of the International Union of Pure and Applied Chemistry (IUPAC), indicating the micropore dominance in the porous structure of the AC. The BET specific surface area of the AC is 2130  $\text{m}^2/\text{g}$ , much higher than that of general commercial AC and other carbon materials, making it conducive to obtaining a high electrosorption capacity. By analyzing the isotherm using density functional theory, the pore size distribution was obtained, as shown in the inset. The curve had two peaks at pore sizes of 1.2 and 1.9 nm, both were micropores. The average pore size of 1.3 nm indicates the micropore dominance in the AC. This pore size was much lower than the thickness of the electrical double layer, indicating the severe overlap of the electrical double layer in the micropore [40]. BET analysis also showed that more than 85% of the specific surface area was contributed by micropores, confirming the micropore dominance in the AC structure.

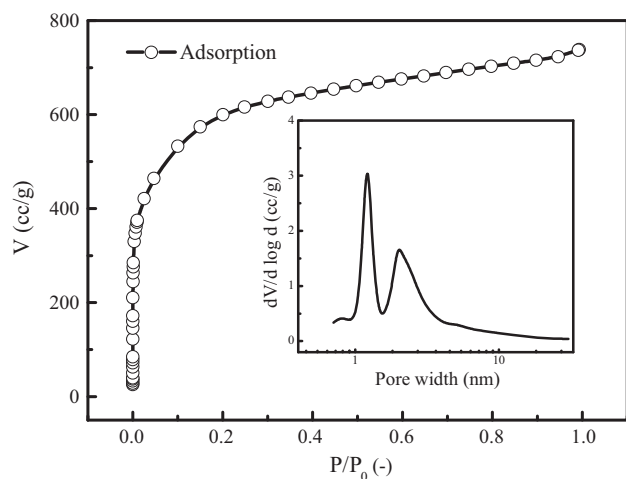


Fig. 2. Nitrogen adsorption isotherm and pore size distribution curve of activated carbon (inset).

The electrochemical performance was evaluated through cyclic voltammetry (CV) curves. The CV curves were measured from  $-0.6$  V to 0 V at different scanning rates ranging from 1 to 50 mV/s using 1 M NaCl aqueous solution, as shown in Fig. 3. The CV curves showed a typical ideal capacitor behavior with a nearly rectangular shape at the lower scanning rate of 1–10 mV/s. As the scanning rate increased to 50 mV/s, the CV curves gradually transformed to a leaf shape, and the capacitance of the AC electrode decreased. For the voltage of  $-0.6$  V and a scanning rate of 1 mV/s, the cell had the capacitance of 140 F/g (AC). For the scanning rate of 5 mV/s, the capacitance is 115 F/g, which is higher than the 75 F/g of the AC electrode (specific area of approximately 900  $\text{m}^2/\text{g}$ ) in the literature under the same operation conditions [19]. The high specific capacitance was attributed to the high specific surface area. However, for the scanning rate of 50 mV/s, the cell had a capacitance of only 75 F/g (AC), little more than half that at 1 mV/s, resulting from the ion diffusion resistance in the micropores. At a high scanning rate, the ions did not have enough time to diffuse into the micropores, leading to decreased capacitance. Fig. 3 also showed that no redox reaction peak occurred at any scanning rate in the CV curves. This indicated that the electrosorption process has no redox reaction, so the process is a non-Faradaic process [22].

#### 3.2. Electrosorption performance of the AC electrodes

The electrosorption performance of the AC electrodes was examined by circulating adsorption under different applied voltages. The initial fluoride concentration was set at 50 mg/L. The applied voltage was increased stepwise from 0 to 1.6 V, and the electrosorption in each step was run for 60 min. The applied voltage was set below 1.6 V for avoiding the possible water electrolysis. After the electrosorption under the 1.6 V step was completed, the electrodes were shorted, and the adsorbed fluoride was released back into the bulk solution. The electrosorption curve is shown in Fig. 4. The AC electrode without voltage applied had no adsorption capacity for fluoride. When the applied voltage was 0.4 V, the electrosorption capacity was still low, likely due to the effects of the electro-capillarity, which determines the threshold voltage of the material response to the applied voltage. When the applied voltage exceeds the threshold voltage, the electrosorption capacity started to increase rapidly [40]. This indicates that the applied voltage of 0.4 V was just slightly higher than the electro-capillarity maximum under this operation condition. A higher elec-

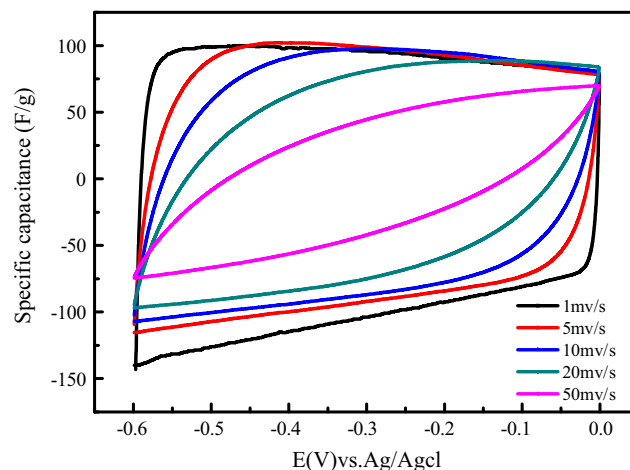


Fig. 3. Cyclic voltammetry characteristic curves of the AC electrode at different scanning rates using 1 M NaCl solution.

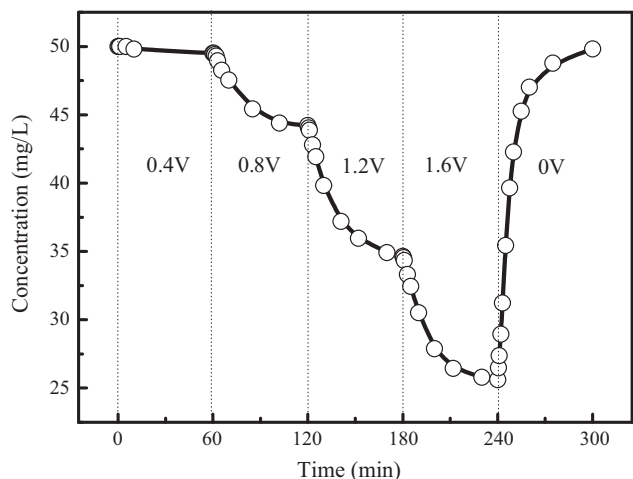


Fig. 4. Electro sorption of fluoride under stepped voltage (initial concentration: 50 mg/L, short-circuit time: 60 min).

trical voltage resulted in a higher electro sorption capacity because of the stronger coulombic force. The similar conclusion was also reported in the research for NaCl removal by using the stepped voltage [25]. When the electro sorption reached equilibrium at a lower voltage, it restarted when a higher voltage was applied, reaching a new equilibrium at a lower fluoride concentration, indicating that the higher applied voltage resulted in a higher electro sorption capacity for fluoride.

For the regeneration of the electrodes, the two electrodes were shorted instead of reversing the applied voltage, to avoid the reverse electro sorption of desorbed ions. When the two electrodes were shorted, the adsorbed fluoride was rapidly released back into the bulk solution due to the lack of electrostatic attraction. After 60 min of desorption, the fluoride concentration of the effluent reached 49.5 mg/L, indicating that 99% of the adsorbed fluoride had been desorbed, representing that the electro sorption is a transient adsorption process. The regeneration process does not need any chemical reagent, making electro sorption a much cleaner and more economical method for fluoride removal compared with conventional adsorption. The high desorption efficiency is because fluoride ions do not react with the functional groups on the AC sur-

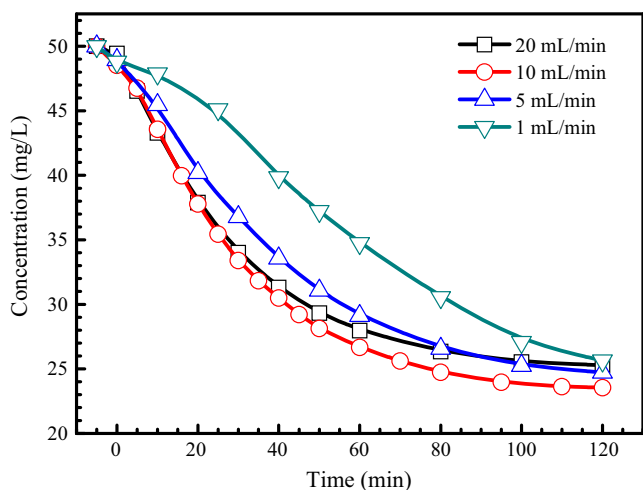


Fig. 5. Fluoride concentration vs time in electro sorption process at different flow rates.

face, so there was no specific adsorption, and all of the fluoride adsorption capacity was contributed by electro sorption.

The fluoride concentration of the water changes with electro sorption time at different flow rates is shown in Fig. 5. The electro sorption efficiency at the flow rate of 10 mL/min was the highest, and it decreased at higher or lower flow rates. For a low flow rate, such as 1 mL/min, the low flow rate of the effluent is the limiting step to decrease the bulk concentration of fluoride, leading to a low electro sorption efficiency. For a high flow rate, the fluoride ions have a short residence time in the cell and do not have sufficient time to diffuse into the micropores, resulting in a high fluoride concentration of the effluent water and low electro sorption efficiency. However, after 120 min electro sorption, all of the electro sorption processes reached equilibrium at fluoride concentrations of almost 25 mg/L for all flow rates, indicating that the equilibrium electro sorption capacities were the same. This means that the flow rate does not change the equilibrium capacity, but affects the electro sorption efficiency. By optimizing the flow rate, the electro sorption can reach equilibrium within the shortest time. Therefore, 10 mL/min was determined to be the optimal flow rate for the highest electro sorption efficiency.

In addition to the applied voltage, the gap between the two electrodes also affects the electro sorption capacity. The gap also affects the volume efficiency of the electro sorption cell. For gaps of 2, 4, and 6 mm, the equilibrium electro sorption capacity for fluoride was 15.1, 14.8 and 13.7 mg/g (AC), respectively, a slightly decreasing trend. This is because the equivalent resistance increased as the gap increased, resulting in a decreased electro sorption capacity. For a more compact electro sorption cell and higher electro sorption capacity, as well as safer operation by avoiding short circuits, 2 mm was determined to be the optimal gap. Therefore, the following experiments were conducted under the optimized conditions, i.e., the applied voltage of 1.6 V, the flow rate of 10 mL/min and the electrode gap of 2 mm.

### 3.3. Isotherm and kinetics of fluoride electro sorption

The electro sorption in each experiment was run for a sufficiently long time to reach equilibrium, and then the electro sorption isotherm of fluoride was obtained, as shown in Fig. 6, from which the saturated electro sorption capacity was determined. The Langmuir and Freundlich models were used to fit the electro sorption isotherm. It is shown that the fitted results conformed better to the Langmuir model, with a correlation coefficient of 0.996, higher than that of the Freundlich model, i.e., 0.900, imply-

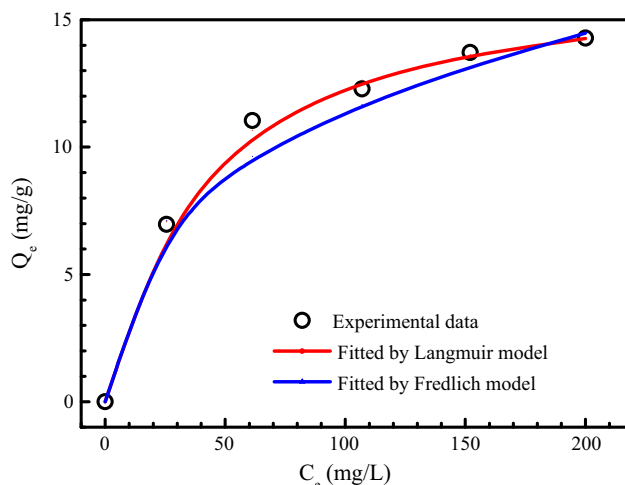


Fig. 6. Electro sorption isotherm fitted with Langmuir and Freundlich models.

ing the monolayer adsorption of fluoride. The fitted parameters are listed in Table 1. The saturated electrosorption capacity for fluoride fitted using the Langmuir model was 16.8 mg/g (AC), which is much higher than that of many natural and synthesized adsorbents, e.g., 0.263 mg/g for montmorillonite, 0.75 mg/g for bone char, 2.41 mg/g for granulated activated alumina and 7 mg/g for granular ferric hydroxide [4]. In addition, neither the electrosorption nor the electrode regeneration uses any chemical reagents, making the process much cleaner and safer. The AC itself had no adsorption capacity for fluoride, but after applying a voltage of 1.6 V, it became an ideal and clean adsorbent for fluoride removal, indicating that electrosorption is an effective method for fluoride removal from water.

The electrosorption performance with an initial fluoride concentration of 50 mg/L under different applied voltages was fitted by a first-order kinetic model, as shown in Table 2. The electrosorption process well conformed to first-order kinetics, with a correlation coefficient higher than 0.98. The equilibrium fluoride concentration is different under different applied voltages. A higher applied voltage resulted in a lower equilibrium concentration  $C_e$ , i.e., a higher equilibrium electrosorption capacity, which resulted from the higher positive charge density for fluoride ions under the higher applied voltage. As the applied voltage increased, the rate constant gradually decreased, which was determined by the structural characteristics of the micropore-dominant AC. In the electrosorption process, the fluoride ions first migrated to the outer surface of the electrode and then diffused into the micropores, after overcoming the diffusion resistance. Because the AC electrodes were of micropore dominance, the internal diffusion was the rate-limiting step in the electrosorption process, and the diffusion resistance is higher in the narrower micropores. As the applied voltage increased, more ions diffused into the narrower pores, so the diffusion resistance was higher, and the rate constant decreased.

The electrosorption results in fluoride removal were also compared with the similar electrosorption process for NaCl removal by using other carbon-based electrodes. The isotherm and kinetics were consistent with many reported literatures, following the Langmuir adsorption isotherm and the pseudo-first-order adsorption kinetics. The Langmuir adsorption capacity for fluoride was 16.8 mg/g (AC), i.e., 0.88 mmol/g. From the literature, the carbon aerogel electrode with a specific surface area of 610 m<sup>2</sup>/g had a Langmuir adsorption capacity of 7 mg/g, i.e., 0.12 mmol/g for NaCl, and the activated carbon fiber electrode with a specific surface area of 670 m<sup>2</sup>/g had a Langmuir adsorption capacity of 8.9 mg/g, i.e., 0.15 mmol/g, and the TiO<sub>2</sub> loaded AC electrode with a specific surface area of 1180 m<sup>2</sup>/g had a Langmuir adsorption capacity of 27.5 mg/g, i.e., 0.47 mmol/g [41]. Gabelich et al. [42] studied the electrosorption for inorganic salts using carbon aerogel with a specific surface area of 400 m<sup>2</sup>/g. For many monovalent salts, e.g., NaCl, KCl and NaNO<sub>3</sub>, with an initial concentration of 5 mmol/L, the carbon aerogel electrodes had the electrosorption capacities in a range of 0.1–0.2 mmol/g. However, the electrosorption capacity for fluoride was 0.58 mmol/g under the similar operation condition in this work. The high electrosorption capacity of the AC

electrode used in this work was attributed to its high specific surface area of 2130 m<sup>2</sup>/g.

### 3.4. Charge efficiency

The current of the electric circuit and the fluoride concentration in the electrosorption process were measured and recorded simultaneously, as shown in Fig. 7. The electric current decreased exponentially, showing a similar changing with the fluoride concentration curve, implying the inherent relativity between the charge transfer and the fluoride removal. The charge efficiency is defined as the amount of ions adsorbed when a unit electron charge is transferred and is used to characterize the efficiency of charge consumption for ion removal [43]. The charge efficiency was calculated using Eq. (3),

$$\eta = \frac{2(C_0 - C_t)VF}{M_F \int_0^t I dt} \quad (3)$$

where  $C_0$  is the initial mass concentration of fluoride (g/L),  $C_t$  is the mass concentration at time  $t$  (g/L),  $F$  is the Faraday constant (C/mol),  $V$  is the solution volume (L),  $M_F$  is the molar mass of fluoride, i.e., 19 g/mol, and  $I$  is the current (A).

Because the electrosorption process is a non-Faradaic process, the electric current is mainly contributed by ion transfer to the reverse electrode. When the electron charge on the electrode is fully compensated by the counterions, the charge efficiency is 1. However, according to the theory of the electrical double layer, counterions and co-ions exist in the electrical double layer. When a voltage is applied on the electrodes, these co-ions are repelled, producing a current that has no contribution to the ion removal, and decreasing the charge efficiency. The charge efficiency was typically around 0.5–0.8, less than 1, due to the co-ions existed in the pores of the carbon electrodes [44].

The charge efficiency versus time is shown in the inset of Fig. 7, indicating that the maximum charge efficiency reached 0.98 at the electrosorption time of 24 min, close to 1. This charge efficiency was much higher than that using other carbon materials. Carbon nanotube electrode with average pore size of 5.0 nm, had a charge efficiency approximately 0.7 [45]. Activated carbon fiber electrode with average pore size of 1.9 nm had a charge efficiency of 0.8 [46]. The AC electrode with average pore size of 1.3 nm in this work reached the highest charge efficiency of 0.98. This indicates that the ion distribution in microporous AC was quite different from that in mesoporous materials, as the co-ions could easily diffuse into mesopores but not into micropores. In the case where only counterions existed in the micropores, there were no co-ions expelled from the pores, so the charge efficiency should be 1. From the molecular dynamics simulations reported in the literature, only counterions existed in pores smaller than 1.1 nm [47]. In this work, the average pore size of the AC was 1.3 nm, which is close to the limit of 1.1 nm and much lower than that in the conventional AC. Because of the tortuosity and irregularity of the micropores in the AC, the diffusion resistance of the co-ions is much higher than that of the counterions, which implies that there are few co-ions in the micropores. Therefore, in the electrosorption process, almost no co-ions were expelled from the electric double layer, enabling

**Table 1**  
Electrosorption isotherm fitted using Langmuir and Freundlich models.

Isotherm	Langmuir			Freundlich		
Model equation	$q = \frac{q_m K_L C}{1 + K_L C}$			$q = K_F C^{1/n}$		
Parameter	$q_m$	$K_L$	$R^2$	$K_F$	$n$	$R^2$
Value	16.8	0.028	0.996	0.847	2.90	0.900

**Table 2**  
Electrosorption kinetics fitted using first-order kinetic model at the flow rate of 10 mL/min.

Kinetic equation	Voltage (V)	R <sup>2</sup>	Ce (mg/L)	k (min <sup>-1</sup> )
$\frac{dC}{dt} = k(C - C_e)$	0.8	0.984	38.6	0.066
	1.2	0.986	27.5	0.057
	1.6	0.990	13.1	0.047

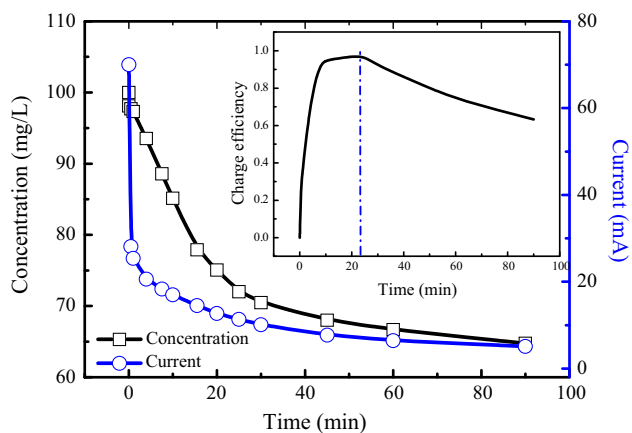


**Fig. 7.** Electrosorption kinetics and charging efficiency (inset).

high charge efficiency. This indicates that the micropore dominance of this AC electrode is beneficial to obtaining high charge efficiency. With the assumption of the charge efficiency as 0.98, for removing 1 mol of fluoride from water, the energy consumption at the applied voltage of 1.6 V was calculated to be 157.6 kJ (0.044 kW·h).

Fig. 7 shows that the fluoride concentration changed slowly, and the current was nearly stable after 40 min. The weak current after 40 min resulted from the ion transfer and the leakage current of the capacitor caused by the solution conductivity. The leakage current was not effective for fluoride removal, so decreased the charge efficiency, as shown in the inset. The charge efficiency decrease in the late stage of the electrosorption was attributed to the leakage current. Because the charge efficiency decreased greatly and the fluoride electrosorption rate was slow in the later period of electrosorption, a long period of electrosorption resulted in a low efficiency. Therefore, the optimal electrosorption time was determined to be 40 min for high electrosorption efficiency.

### 3.5. Saturated electrosorption capacity

The saturated electrosorption capacity at applied voltages ranging from 0.2 to 1.6 V was measured, as shown in Fig. 8. The saturated electrosorption capacity had a good linear relationship with the square of the voltage, with a squared correlation coefficient of 0.996. The fitted line had an intercept of 0.14 V at the voltage axis, indicating that the maximum voltage of the electro-capillarity was 0.14 V, i.e., the electrosorption occurs only when the applied voltage was higher than this value. This confirms the existence of the electro-capillarity, as shown in Fig. 4.

The discussion in Section 3.4 indicates that there existed few co-ions inside the micropores. Assuming that only counterions existed in the micropore, according to the deduction from the Poisson - Boltzmann equation [48],

$$\rho_s = \rho_0 + \sigma^2 / 2\epsilon\epsilon_0 kT \quad (4)$$

where  $\rho_s$  is the density of fluoride ions adsorbed on the electrode surface (number/m<sup>3</sup>),  $\rho_0$  is the density in the bulk solution (num-

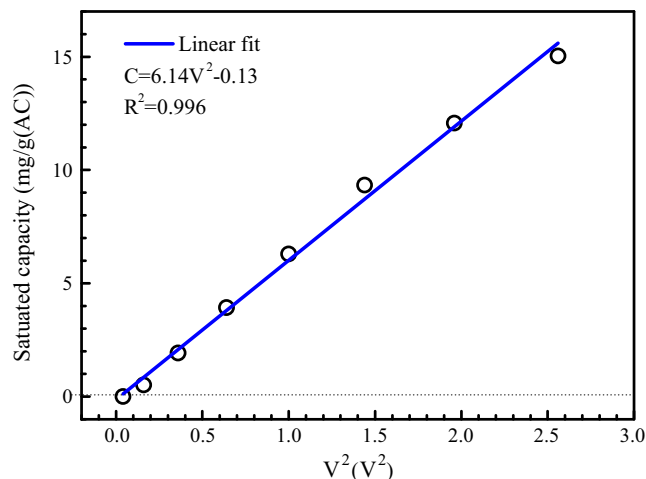


**Fig. 8.** Linear relationship between saturated electrosorption capacity and the square of the voltage.

ber/m<sup>3</sup>),  $\sigma$  is the surface charge density (C/m<sup>2</sup>),  $\epsilon$  is the dielectric constant (-),  $\epsilon_0$  is the vacuum dielectric constant (F/m),  $T$  is the temperature of the solution (K), and  $k$  is the Boltzmann constant (J/K).

Because the fluoride ions were highly condensed on the electrode surface in the electrosorption process,  $\rho_s$  was much higher than  $\rho_0$ , so  $\rho_0$  could be neglected in Eq. (4). Hence, the density of fluoride ions on the electrode surface  $\rho_s$  was proportional to the surface charge density  $\sigma^2$ ,

$$\rho_s \propto \sigma^2 \quad (5)$$

The literature reports that the surface charge density was nearly proportional to the surface potential [36,49], so that

$$\rho_s \propto U^2 \quad (6)$$

Because the average pore size of this micropore-dominant AC was 1.3 nm, and the hydration diameter of the fluoride ions was 0.704 nm, so the space in the micropores is not sufficient for the formation of an electrical double layer. It was inferred that the fluoride ions in the micropores were adsorbed in the monolayer, which is consistent with the fitted Langmuir model of the electrosorption isotherm, i.e., the monolayer adsorption. Because the adsorption only occurs on the surface, the electrosorption capacity for fluoride was determined by the  $\rho_s$  in Eq. (6). Therefore, for the case where only counterions exist in the micropores, the saturated electrosorption capacity had a linear relationship with the square of the voltage, which is consistent with the experimental results, as shown in Fig. 8.

## 4. Conclusions

An electrosorption process using micropore-dominant AC as the electrode material for fluoride removal was developed, and the results were compared with NaCl removal by other carbon-based electrodes. The applied voltage, flow rate and the gap of the electrodes were optimized for high electrosorption efficiency. The high

saturated electrosorption capacity of 16.8 mg/g for fluoride was attributed to its high specific area of 2130 m<sup>2</sup>/g, and the electrosorption isotherm conforms to the Langmuir model, i.e., monolayer adsorption. The saturated electrosorption capacity has a good linear relationship with the square of the voltage. The electrosorption of fluoride ions occurs only when the applied voltage is higher than the electro-capillary maximum, 0.14 V for the micropore-dominant AC. The micropores hold few co-ions because of the narrow pore size of the AC, and the micropore dominance is beneficial to increasing the charge efficiency, which reaches 0.98 in this work. The electrodes are easily completely regenerated by shorting. The electrosorption shows a promising future for the fluoride removal from water.

## Acknowledgements

The authors wish to express their appreciation for the financial support of this study by the National High Technology Research and Development Program (863 Program, No. 2012AA062605) and the National Natural Science Foundation of China (NSFC No. 21176134).

## References

- [1] V. Tomar, D. Kumar, A critical study on efficiency of different materials for fluoride removal from aqueous media, *Chem. Cent. J.* 7 (2013) 1–15.
- [2] L. Chen, H.X. Wu, T.J. Wang, Y. Jin, Y. Zhang, X.M. Dou, Granulation of Fe–Al–Ce nano-adsorbent for fluoride removal from drinking water by spray coating on sand in a fluidized bed, *Powder Technol.* 193 (2009) 59–64.
- [3] WHO, in: *Guidelines for Drinking Water Quality*, Geneva, 2004.
- [4] A. Bhatnagar, E. Kumar, M. Sillanpää, Fluoride removal from water by adsorption - a review, *Chem. Eng. J.* 171 (2011) 811–840.
- [5] E. Vences-Alvarez, L.H. Velazquez-Jimenez, L.F. Chazaro-Ruiz, P.E. Diaz-Flores, J.R. Rangel-Mendez, Fluoride removal in water by a hybrid adsorbent lanthanum–carbon, *J. Colloid Interface Sci.* 455 (2015) 194–202.
- [6] L. Chen, B.Y. He, S. He, T.J. Wang, C.L. Su, Y. Jin, Fe–Ti oxide nano-adsorbent synthesized by co-precipitation for fluoride removal from drinking water and its adsorption mechanism, *Powder Technol.* 227 (2012) 3–8.
- [7] M. Mohapatra, S. Anand, B.K. Mishra, D.E. Giles, P. Singh, Review of fluoride removal from drinking water, *J. Environ. Manage.* 91 (2009) 67–77.
- [8] X. Fan, D.J. Parker, M.D. Smith, Adsorption kinetics of fluoride on low cost materials, *Water Res.* 37 (2003) 4929–4937.
- [9] S.G. Wang, Y. Ma, Y.J. Shi, W.X. Gong, Defluoridation performance and mechanism of nano-scale aluminum oxide hydroxide in aqueous solution, *J. Chem. Technol. Biot.* 84 (2009) 1043–1050.
- [10] E. Kumar, A. Bhatnagar, M. Ji, W. Jung, S.H. Lee, S.J. Kim, G. Lee, H. Song, J.Y. Choi, J.S. Yang, B.H. Jeon, Defluoridation from aqueous solutions by granular ferric hydroxide (GFH), *Water Res.* 43 (2009) 490–498.
- [11] K. Biswas, K. Gupta, U.C. Ghosh, Adsorption of fluoride by hydrous iron (III)-tin (IV) bimetal mixed oxide from the aqueous solutions, *Chem. Eng. J.* 149 (2009) 196–206.
- [12] X. Dou, Y. Zhang, H. Wang, Y. Wang, Performance of granular zirconium-iron oxide in the removal of fluoride from drinking water, *Water Res.* 45 (2011) 3571–3578.
- [13] K. Biswas, S. Debnath, U.C. Ghosh, Physicochemical aspects on fluoride adsorption for removal from water by synthetic hydrous iron(III)-chromium (III) mixed oxide, *Sep. Sci. Technol.* 45 (2010) 472–485.
- [14] B. Zhao, Y. Zhang, X. Dou, X. Wu, M. Yang, Granulation of Fe–Al–Ce trimetal hydroxide as a fluoride adsorbent using the extrusion method, *Chem. Eng. J.* 185 (2012) 211–218.
- [15] S.B. Deng, Z.J. Li, J. Huang, G. Yu, Preparation, characterization and application of a Ce–Ti oxide adsorbent for enhanced removal of arsenate from water, *J. Hazard. Mater.* 179 (2010) 1014–1021.
- [16] S. Deng, H. Liu, W. Zhou, J. Huang, G. Yu, Mn–Ce oxide as a high-capacity adsorbent for fluoride removal from water, *J. Hazard. Mater.* 186 (2011) 1360–1366.
- [17] Meenakshi, R.C. Maheshwari, Fluoride in drinking water and its removal, *J. Hazard. Mater.* 137 (2006) 456–463.
- [18] L. Chao, Z. Liu, G. Zhang, X.N. Song, X.D. Lei, M. Noyong, U. Simon, Z. Chang, X. M. Sun, Enhancement of capacitive deionization capacity of hierarchical porous carbon, *J. Mater. Chem. A* 3 (2015) 12730–12737.
- [19] C.H. Hou, C.Y. Huang, A comparative study of electrosorption selectivity of ions by activated carbon electrodes in capacitive deionization, *Desalination* 314 (2013) 124–129.
- [20] Z. Chen, H. Zhang, C. Wu, Y. Wang, W. Li, A study of electrosorption selectivity of anions by activated carbon electrodes in capacitive deionization, *Desalination* 369 (2015) 46–50.
- [21] J.H. Choi, Fabrication of a carbon electrode using activated carbon powder and application to the capacitive deionization process, *Sep. Purif. Technol.* 70 (2010) 362–366.
- [22] G. Wang, C. Pan, L. Wang, Q. Dong, C. Yu, Z.B. Zhao, J.S. Qiu, Activated carbon nanofiber webs made by electrospinning for capacitive deionization, *Electrochim. Acta* 69 (2012) 65–70.
- [23] Y. Chen, M. Yue, Z.H. Huang, F. Kang, Electrospun carbon nanofiber networks from phenolic resin for capacitive deionization, *Chem. Eng. J.* 252 (2014) 30–37.
- [24] P. Xu, J.E. Drewes, D. Heil, G. Wang, Treatment of brackish produced water using carbon aerogel-based capacitive deionization technology, *Water Res.* 42 (2008) 2605–2617.
- [25] C.H. Hou, N.L. Liu, H.L. Hsu, W. Den, Development of multi-walled carbon nanotube/poly (vinyl alcohol) composite as electrode for capacitive deionization, *Sep. Purif. Technol.* 130 (2014) 7–14.
- [26] H. Li, T. Lu, L. Pan, Y. Zhang, Z. Sun, Electrosorption behavior of graphene in NaCl solutions, *J. Mater. Chem.* 19 (2009) 6773–6779.
- [27] H.B. Li, L.D. Zou, L.K. Pan, Z. Sun, Novel graphene-like electrodes for capacitive deionization, *Environ. Sci. Technol.* 44 (2010) 8692–8697.
- [28] C. Tsouris, R. Mayes, J. Kiggans, K. Sharma, S. Yiacoumi, D. DePaoli, S. Dai, Mesoporous carbon for capacitive deionization of saline water, *Environ. Sci. Technol.* 45 (2011) 10243–10249.
- [29] D. Zhang, X. Wen, L. Shi, T. Yan, J. Zhang, Enhanced capacitive deionization of graphene/mesoporous carbon composites, *Nanoscale* 4 (2012) 5440–5446.
- [30] Z. Peng, D. Zhang, L. Shi, T. Yan, High performance ordered mesoporous carbon/carbon nanotube composite electrodes for capacitive deionization, *J. Mater. Chem.* 22 (2012) 6603–6612.
- [31] S. Porada, L. Borchardt, M. Oschatz, M. Bryjak, J.S. Atchison, K.J. Keesman, S. Kaskel, P.M. Biesheuvel, V. Presser, Direct prediction of the desalination performance of porous carbon electrodes for capacitive deionization, *Energy Environ. Sci.* 6 (2013) 3700–3712.
- [32] J. Lee, S. Kim, C. Kim, J. Yoon, Hybrid capacitive deionization to enhance the desalination performance of capacitive techniques, *Energy Environ. Sci.* 7 (2014) 3683–3689.
- [33] J.C. Farmer, S.M. Bahowick, J.E. Harrar, D.V. Fix, R.E. Martinelli, A.K. Vu, K.L. Carroll, Electrosorption of chromium ions on carbon aerogel electrodes as a means of remediating ground water, *Energy Fuel* 11 (1997) 337–347.
- [34] S.Y. Huang, C.S. Fan, C.H. Hou, Electro-enhanced removal of copper ions from aqueous solutions by capacitive deionization, *J. Hazard. Mater.* 278 (2014) 8–15.
- [35] H. Li, L. Zou, L. Pan, Z. Sun, Using graphene nano-flakes as electrodes to remove ferric ions by capacitive deionization, *Sep. Purif. Technol.* 75 (2010) 8–14.
- [36] J.C. Farmer, D.V. Fix, G.V. Mack, R.W. Pekala, J.F. Poco, Capacitive deionization of NaCl and NaNO<sub>3</sub> solutions with carbon aerogel electrodes, *J. Electrochem. Soc.* 143 (1996) 159–169.
- [37] W. Tang, P. Kovalsky, D. He, T.D. Waite, Fluoride and nitrate removal from brackish groundwaters by batch-mode capacitive deionization, *Water Res.* 84 (2015) 342–349.
- [38] L. Han, K.G. Karthikeyan, M.A. Anderson, K.B. Gregory, Exploring the impact of pore size distribution on the performance of carbon electrodes for capacitive deionization, *J. Colloid Interface Sci.* 430 (2014) 93–99.
- [39] G. Wang, Q. Dong, Z. Ling, C. Pan, C. Yu, J.S. Qiu, Hierarchical activated carbon nanofiber webs with tuned structure fabricated by electrospinning for capacitive deionization, *J. Mater. Chem.* 22 (2012) 21819–21823.
- [40] K.L. Yang, T.Y. Ying, S. Yiacoumi, C. Tsouris, E.S. Vittoratos, Electrosorption of ions from aqueous solutions by carbon aerogel: an electrical double-layer model, *Langmuir* 17 (2001) 1961–1969.
- [41] L. Wang, M. Wang, Z.H. Huang, T. Cui, X. Gui, F. Kang, K. Wang, D. Wu, Capacitive deionization of NaCl solutions using carbon nanotube sponge electrodes, *J. Mater. Chem.* 21 (2011) 18295–18299.
- [42] C.J. Gabelich, T.D. Tran, I.H. Suffet, Electrosorption of inorganic salts from aqueous solution using carbon aerogels, *Environ. Sci. Technol.* 36 (2002) 3010–3019.
- [43] L. Zou, L. Li, H. Song, G. Morris, Using mesoporous carbon electrodes for brackish water desalination, *Water Res.* 42 (2008) 2340–2348.
- [44] T. Kim, J.E. Dykstra, S. Porada, A. van der Wal, J. Yoon, P.M. Biesheuvel, Enhanced charge efficiency and reduced energy use in capacitive deionization by increasing the discharge voltage, *J. Colloid Interface Sci.* 446 (2014) 317–326.
- [45] H. Li, S. Liang, M. Gao, G. Li, J. Li, L. He, The study of capacitive deionization behavior of a carbon nanotube electrode from the perspective of charge efficiency, *Water Sci. Technol.* 71 (2015) 83–88.
- [46] Z.H. Huang, M. Wang, L. Wang, L. Kang, Relation between the charge efficiency of activated carbon fiber and its desalination performance, *Langmuir* 28 (2012) 5079–5084.
- [47] Y. Shim, H.J. Kim, Nanoporous carbon supercapacitors in an ionic liquid: a computer simulation study, *ACS Nano* 4 (2010) 2345–2355.
- [48] J.N. Israelachvili, *Intermolecular and Surface Forces*, third ed., Academic Press, 2011, Reference to a chapter in an edited book: 14–4.
- [49] P.M. Biesheuvel, Thermodynamic cycle analysis for capacitive deionization, *J. Colloid Interface Sci.* 332 (2009) 258–264.